UNIVERSITY OF CALIFORNIA SAN DIEGO

The Potential Effect of Chitin on Lung Inflammation and Lung Cancer Progression in Mice

A thesis submitted in partial satisfaction of the
requirements for the degree Master of Science

in

Biology

by

Sneha Ganguly

Committee in charge:

Professor Eyal Raz, Chair
Professor Enfu Hui, Co-Chair
Professor Matthew Daugherty

2022

The thesis of Sneha Ganguly is approved, and it is acceptable in quality and form for publication on microfilm and electronically.

University of California San Diego

2022

TABLE OF CONTENTS

LIST OF FIGURES

LIST OF TABLES

ACKNOWLEDGEMENTS

I would like to express my biggest gratitude to my Principal Investigator and my Thesis Advisor, Dr. Eyal Raz, for providing me with help and guidance throughout my undergraduate and graduate career at UC San Diego and for constantly exposing me to the exciting world of immunology. I would also like to express my gratitude to my project mentor, Dr. Samuel Bertin, for all the immense knowledge he has provided me over my time at the lab, for tirelessly helping me sort through my data and analyze it, picking my brain for new experimental ideas at every step of the way, for being a constant guide, and teaching me how to be a researcher. I would also like to thank my fellow lab members Lauren Amaya, Liping Zeng, Lindsey Griffin, Han Chang, Dongjie Wang, and David Herdman for helping me with the experiments and data collection for my thesis, without whom my research journey would not have been as fulfilling.

Figure 1 is currently being prepared for submission for publication of the material. Wang, Dong-Jie; Ganguly, Sneha; Bertin, Samuel. “Chronic Exposure to House Dust Mites Accelerates Lung Cancer Progression in Mice by Activating the NLRP3/IL-1β Pathway in Lung Macrophages.” The thesis author was the co-author of this material.

Figure 2 is currently being prepared for submission for publication of the material. Wang, Dong-Jie; Ganguly, Sneha; Bertin, Samuel. “Chronic Exposure to House Dust Mites Accelerates Lung Cancer Progression in Mice by Activating the NLRP3/IL-1β Pathway in Lung Macrophages.” The thesis author was the co-author of this material.

Figure 3 is currently being prepared for submission for publication of the material. Wang, Dong-Jie; Ganguly, Sneha; Bertin, Samuel. “Chronic Exposure to House Dust Mites Accelerates Lung Cancer Progression in Mice by Activating the NLRP3/IL-1β Pathway in Lung Macrophages.” The thesis author was the co-author of this material.

ABSTRACT OF THE THESIS

The Potential Effect of Chitin on Lung Inflammation and Lung Cancer Progression in Mice

by

Sneha Ganguly

Master of Science in Biology

University of California San Diego, 2022

Professor Eyal Raz, Chair
Professor Enfu Hui, Co-Chair

Previous investigations in the laboratory demonstrated that chronic exposure to house dust mites (HDM), a common indoor aeroallergen associated with the development of asthma, accelerates lung cancer (LC) development in mice. The tumor-promoting effect of HDM was

mainly due to NLRP3 inflammasome activation in macrophages and increased IL-1β production as the blockade of these molecules abrogated the effect of HDM on tumor development. Interestingly, the lung tumor-promoting effect of HDM was not completely abolished by heat treatment of the HDM extract, suggesting that the heat-insensitive factors play a role in its pro-tumorigenic effect. Chitin, a component of the HDM exoskeleton, is an abundant 1,4-beta blinked N-glucosamine polymer that is rigid and hard to degrade. Here we performed additional mechanistic studies using the RAW 264.7 mouse macrophage cell line and bone marrow-derived macrophages (BMDMs), and investigated the specific effect of chitin, a major constituent of HDM, on IL-1β production. We also test the effect of chronic exposure to chitin on LC development in a genetically engineered mouse model (GEMM) of mutated KRAS.

INTRODUCTION

Lung cancer is one of the leading causes of cancer-related deaths in men and women worldwide [2]. While it is well known that tobacco smoking is one of the primary risk factors for lung cancer, up to 25% of all lung cancer deaths are patients without any smoking history [2]. Chronic inflammation has been linked to the development of various diseases including cancer [2,25]. In the lungs, chronic inflammation as occurring in certain lung diseases such as asthma is also associated with an increased risk of developing lung cancer [2]. One of the most prominent pathologies of asthma is the hyper inflammation of the lung airway in response to environmental allergic triggers [3]. This allergic response is marked by inflammation of the lung airway epithelium, super secretion of mucus from the lung epithelial cells, especially in the bronchioles, and a constriction of the airway because of the inflammatory response [3]. However, the association between asthma and lung cancer is controversial and the type or subtypes of inflammation that drive tumor development remains unknown.

House Dust Mites (HDM) contain multiple allergenic and bioactive molecules that can provoke lung epithelium damage [6] and HDM was shown to induce DNA damage in lung epithelial cells [7, 8]. In addition, in previous studies, we identified that chronic HDM exposure also induces the production of the pro-inflammatory cytokine IL-1β in the lungs by macrophages and accelerates lung tumor development in two different mouse models of lung cancer [9]. To better understand the pro-tumorigenic effect that HDM plays, one must understand its constituents. Among them, Der p and Der f, found in *Dermatophagoides pteronyssinus* and *Dermatophagoides farinae*, the two most prevalent HDM species, are active cysteine proteases highly concentrated in HDM fecal matter [10]. This fecal matter is airborne and as such is easily inhalable when humans make contact with their furniture, bedding, and pillows [11]. In addition

to Der p and Der f allergens, the mite bodies themselves can also be inhaled and their various components can activate both innate and adaptive immunity. The mites' exoskeleton is comprised of chitin, fungal spores, and associated bacteria which contain LPS [6]. The chitin comprises most of the fungal exoskeleton as well as a considerable portion of the fecal matter and acts as an adjuvant and influences both adaptive Th1, Th2, and Th17 immunity and innate immunity [6,12].

Chitin is an abundant 1,4-beta blinked N-glucosamine polymer that is rigid and hard to degrade [7]. Mammalians do not produce chitin but act as hosts for several chitin-containing microorganisms, making it a substance that is tagged as a pathogen-associated molecular pattern (PAMP) for the immune system [12]. Primarily detected in the lungs, chitin is known to activate various innate and adaptive immune responses, including cytokine production and macrophage activation that results in inflammation [12,13]. When HDM enters mammalian lungs via inhalation, the chitinaceous exoskeleton is very hard to digest [6,7]. However, mammals have chitin-binding enzymes known as chitinases, which can break the hydrogen bonds between the chitin monomers and digest them [8]. One of the better known and more potent chitinases is known as the acidic mammalian chitinase or AMCase [12]. AMCase is produced by the lung epithelial cells when they detect chitin via dectin receptors on the cell surface [14]. AMCase is also produced by macrophages when they detect chitin via the Toll-like receptors 2 (TLR2) [14]. However, even with the production of AMCase, large fragments of chitin that remain undigested are not always entirely cleared away via macrophage phagocytosis and these fragments can accumulate in the lungs to cause inflammation [8].

Inflammation in the lungs is regulated by a balance of pro- or anti-inflammatory cytokines and chemokines. Chemokines have a key role in the recruitment of immune cells such as macrophages, monocytes, neutrophils, eosinophils, mast cells, and B and T cells to the site of

inflammation [15]. These cells, in turn, secrete various other cytokines that induce phagocytosis or enzymatic degradation of pathogens, having meticulous control on immunomodulation at the site of infection [15]. Some of the commonly known pro-inflammatory cytokines found at the site of infection are IL-1β, IL-6, and TNF; they are well-known activators of macrophages that perform phagocytosis and remove the infection-causing pathogen fragments from the site of inflammation [15, 16].

Among these pro-inflammatory cytokines, IL-1β is essential in regulating immune responses to infection [16]. In macrophages, IL-1β is expressed as an inactive proenzyme which is activated following cleavage of the pro-form by caspase-1 [17]. The activity of caspase-1 is regulated mainly by the inflammasome Nod-like receptor family pyrin domain-containing protein 3 (NLRP3) [17]. NLRP3 is a pattern recognition receptor (PRR) that detects PAMPs like chitin [18]. The activation of NLRP3 requires a two-step priming signal; the first one increases the expression of the PRR on the cell surface and the expression of proenzyme pro-IL-1β, and the second priming signal induces the formation of the inflammasome, activation of caspase-1, and the cleavage of pro-IL-1β to form IL-1β [17,18]. Then mature IL-1β is released from the cells and activates other inflammatory pathways [17,18]. Recent studies have shown increased NLRP3 activation and IL-1β production in patients with non-small cell lung cancer [19]. Moreover, we have also found that the tumor-promoting effect of HDM was mainly due to the chronic activation of the NLRP3 inflammasome in lung macrophages and increased production of IL-1β as the blockade of these molecules abrogated this effect [1].

Hence, we investigate whether chitin contributes to the production of IL-1β in response to HDM exposure and to its pro-tumorigenic effect. To address these questions, we utilized $CCSP^{Cre+/-}Kras^{G12D+/-}$ mice (hereafter referred to as $Kras^{G12D}$ mice), which develop spontaneous lung tumors [20] and mirrored KRAS-mutated human ACs [21]. We also utilized the RAW264.7

murine macrophage cell line as well as bone marrow-derived macrophages (BMDMs) to determine the effects that chitin has on IL-1β production *in vitro* and understand whether chitin can activate the inflammasome. Our data indicate that chitin stimulates IL-1β production and therefore suggests that it is able to activate NLRP3 similar to LPS that we used as a positive control. These studies indicate that chitin induces IL-1β secretion by macrophages in a dose-dependent manner *in vitro* as well as leads to inflammation and acceleration of lung cancer development *in vivo*.

RESULTS

Chronic exposure to HDM accelerates LC progression in a mutant *Kras*-driven LC mouse model *Kras^{G12D}*

To evaluate the effect of chronic HDM exposure on LC development, we used a *Kras^{G12D}* mouse model which spontaneously develops tumors in the lung [20]. The reason we used this model is that having a mutated KRAS is one of the most common promoters in NSCLC and confers a poor prognosis, thereby allowing us to evaluate the potential clinical effect of HDM [21]. We treated *Kras^{G12D}* mice intranasally with HDM or VEH for 9 weeks and evaluated the occurrence of both lung inflammation as well as lung tumors in the groups at 14 weeks of age. The lungs of the HDM-treated *Kras^{G12D}* mice were found to be larger and heavier than that of the vehicle-treated mice (data not shown). Furthermore, administration of HDM was found to significantly increase the number of lung lesions, including mainly alveolar/bronchiolar hyperplasia, adenomas, and less frequently adenocarcinomas as well as the tumor area in the *Kras^{G12D}* mice when compared to the control mice (data not shown).

Since HDM is an allergenic mixture that contains various proteases which are known to invoke lung epithelial damage [22], we compared the effects of proteolytically active HDM and heat-inactivated HDM (HI-HDM, 1h at 95 °C) [23] to those of the control vehicle. To understand the effect that HDM has on tumor progression and to gauge the contribution of HDM-derived proteases, we treated another cohort of *Kras^{G12D}* mice intranasally with HDM, HI-HDM, or VEH for 9 weeks followed by an additional 4 weeks without intranasal treatment allowing the tumor to grow and analyzing the number and sub-type of lung tumors in the experimental groups at 18 weeks age (Fig 1A). Analysis of H&E stained showed the presence of dense perivascular and peribronchial mononuclear inflammatory infiltrates in the lungs of the HDM-treated mice (Fig

1B). These features of inflammation were reduced in HI-HDM-treated mice and almost absent in the lungs of the VEH-treated mice (Fig 1B). The analysis also found that mice treated with HDM, but not HI-HDM, had significantly increased tumor multiplicity and tumor area when compared to the VEH mice (Fig 1C and 1D).

The lesions found in the lungs of HDM-treated mice observed more high-grade lesions compared to the VEH-treated mice while HI-HDM-treated mice lungs showed no significant differences when compared to HDM or VEH-treated mice (data not shown). Overall, these results suggest that chronic exposure to HDM accelerates the progression of the lung lesions from hyperplasia to adenoma and adenocarcinoma in a $Kras^{G12D}$-driven mouse model and that heat-sensitive factors in HDM extracts contribute to this effect.

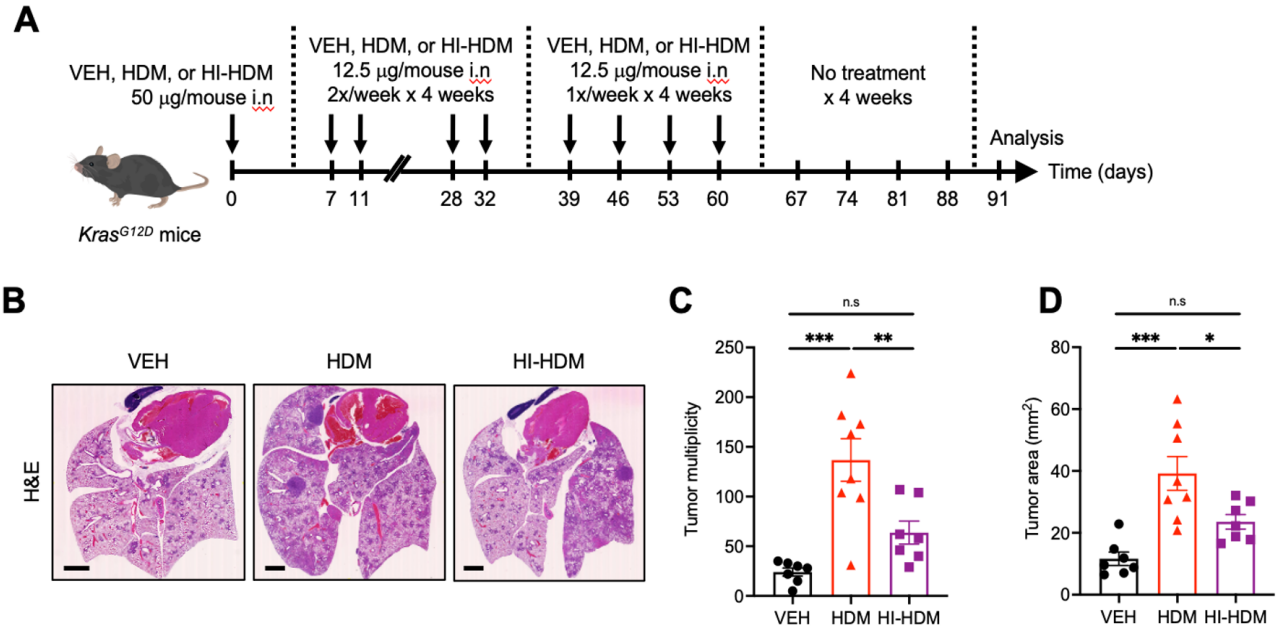

Figure 1: Chronic exposure to HDM accelerates lung cancer progression in a *Kras*^{G12D}-driven mouse model and heat-sensitive factors in HDM extract contribute to this effect A) Five-week-old *Kras*^{G12D} mice were randomly assigned to three groups and were treated i.n with VEH (n = 7), HDM (n = 8), or HI-HDM (n = 7) for 13 weeks as indicated in this schematic overview of the study design. **B)** Representative pictures of H&E-stained lung sections of mice treated with VEH, HDM, or HI-HDM. Scale bars, 2 mm. **C)** Tumor multiplicity (i.e., number of lung lesions per mouse) was calculated on H&E-stained sections as shown in B. **D)** Tumor area (i.e., the sum of lesion surface areas per mouse) was calculated on H&E-stained sections as shown in B using QuPath software. Data are presented as mean ± SEM. Statistical significance was assessed by one-way ANOVA with post hoc Bonferroni's test. (n.s: not significant, * $P < 0.05$, ** $P < 0.01$, *** $P < 0.001$).

Exposure to HDM induces IL-1β production by mouse macrophages

Recently, studies have suggested that the activation of the NLRP3 inflammasome and the consequent increase in IL-1β production are associated with tumor progression in various cancer types, including LC [24]. Therefore, we wanted to assess the possible activation of the IL-1β signaling pathway in the lungs of mice treated with HDM, HI-HDM, or VEH. We found increased production of mature IL-1β in immunoblotting as well as enzyme-linked immunosorbent assays (ELISA) in lung tissue homogenates of $Kras^{G12D}$ mice treated with HDM, lesser in HI-HDM, and almost negligible in VEH-treated mice (data not shown). The fact that IL-1β expression consistently remained elevated in the lung tissue even four weeks after the last intranasal challenge, suggests that the IL-1β signaling pathway is persistently activated by HDM.

Because macrophages are known to be a major cell type that produces IL-1β via the activation of the NLRP3 inflammasome, we wanted to focus our studies on macrophages [25]. To determine whether HDM directly induces IL-1β production by macrophages, we conducted *in vitro* cell-based assays with primary bone marrow-derived macrophages (BMDMs). We isolated the BMDMs from WT C57BL/6 mice and stimulated them for 24h with HDM, HI-HDM, or VEH in the presence of extracellular ATP, and IL-1β secretion in the supernatants was measured by ELISA (Fig 2A). Similar to what was seen in the lung tissues, HDM stimulation led to a significant increase in IL-1β, compared to the lower expression of IL-1β in the culture supernatants of HI-HDM-treated and VEH-treated BMDM cells. Therefore, this data shows that HDM-derived proteases activate the IL-1β signaling pathway in macrophages and by doing so might be creating a pro-tumor lung microenvironment.

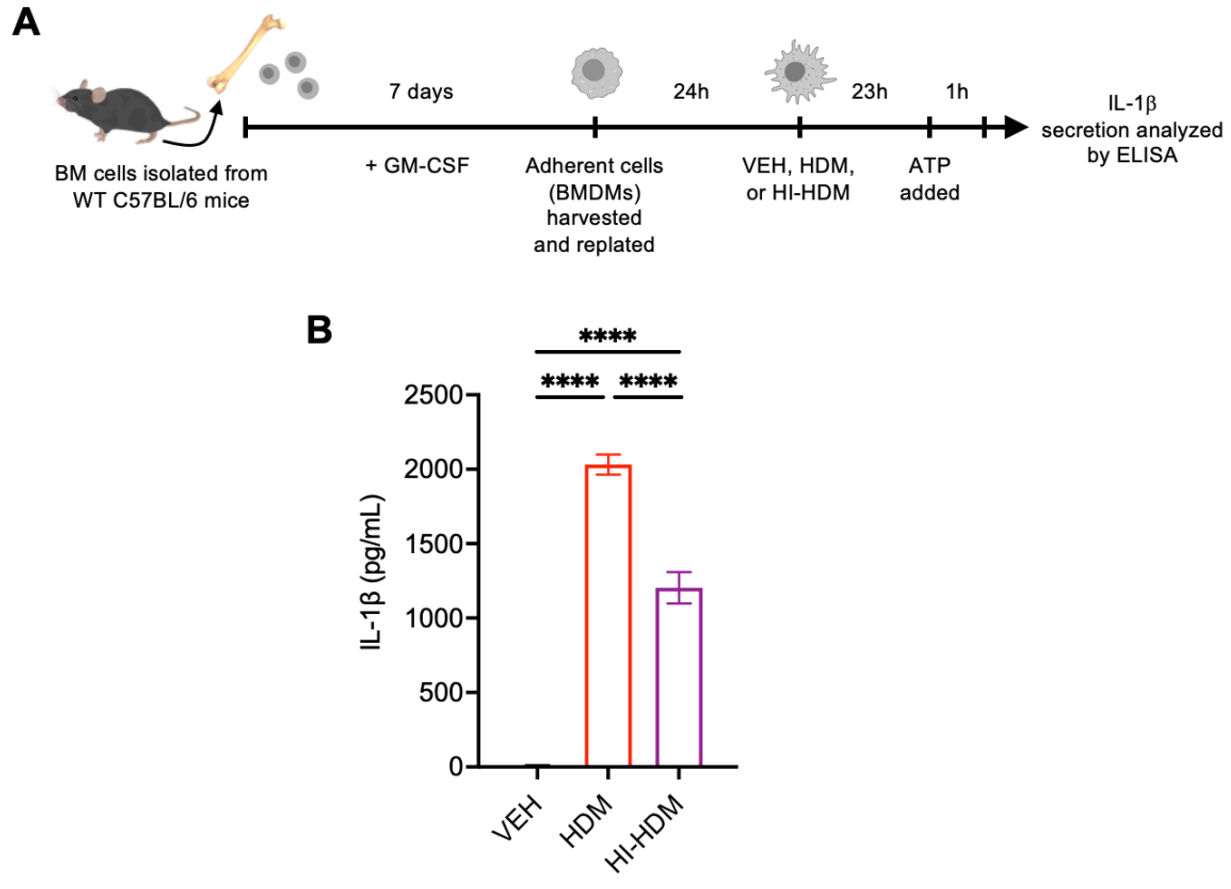

Figure 2: HDM induces IL-1β production by mouse macrophages and both heat-sensitive and -insensitive factors in HDM extract contribute to this effect A) Schematic overview of the BMDM culture system. Bone marrow (BM) cells were harvested from wild-type (WT) mice and were differentiated into bone marrow-derived macrophages (BMDMs) in presence of granulocyte-macrophage colony-stimulating factor (GM-CSF) for 7 days. **B)** WT BMDMs were stimulated for 24h with VEH (PBS), HDM, or HI-HDM, both 200 µg/mL, and ATP (5 mM) was added to each well for the last hour of culture. The supernatants were collected and the levels of IL-1β were analyzed by ELISA. Data are presented as mean ± SEM. Statistical significance was assessed by one-way ANOVA with post hoc Bonferroni's test. (**** $P < 0.0001$).

Neutralization of IL-1β or CCL2 inhibited the tumor-promoting effect of HDM

Based on our data that HDM induces IL-1β production in macrophages in the lungs, we hypothesized that the IL-1β pathway is the primary pathway that drives LC progression in response to chronic HDM exposure in our *Kras*^{G12D} mouse model. To test our hypothesis, we treated *Kras*^{G12D} mice with HDM or VEH intranasally and either IL-1β Ab or isotype control Ab

intraperitoneally and determined the effect on tumor progression (Fig 3A). It has been previously reported that IL-1β neutralization did not affect spontaneous tumor formation in *Kras*^{G12D} mice, but interestingly, IL-1β neutralization completely abolished the tumor-promoting effect of HDM (Fig 3C). Moreover, mice treated with HDM and anti-IL-1β Ab had more grade 1 but fewer grade 2 lesions than the mice treated with HDM and isotype control Ab (Fig 3B). We also hypothesized that blocking the activity of a key IL-1β target gene such as CCL2 would show a similar result as the anti-IL-1β Ab in *Kras*^{G12D} mice. As expected, blocking CCL2 almost completely stopped the effect of HDM on tumor development and progression (Fig 3B and 3C). Hence, these data suggest that the tumor-promoting effect of HDM in the lungs is mostly mediated by the activation of the IL-1β signaling pathway in the macrophage cells recruited to the lungs.

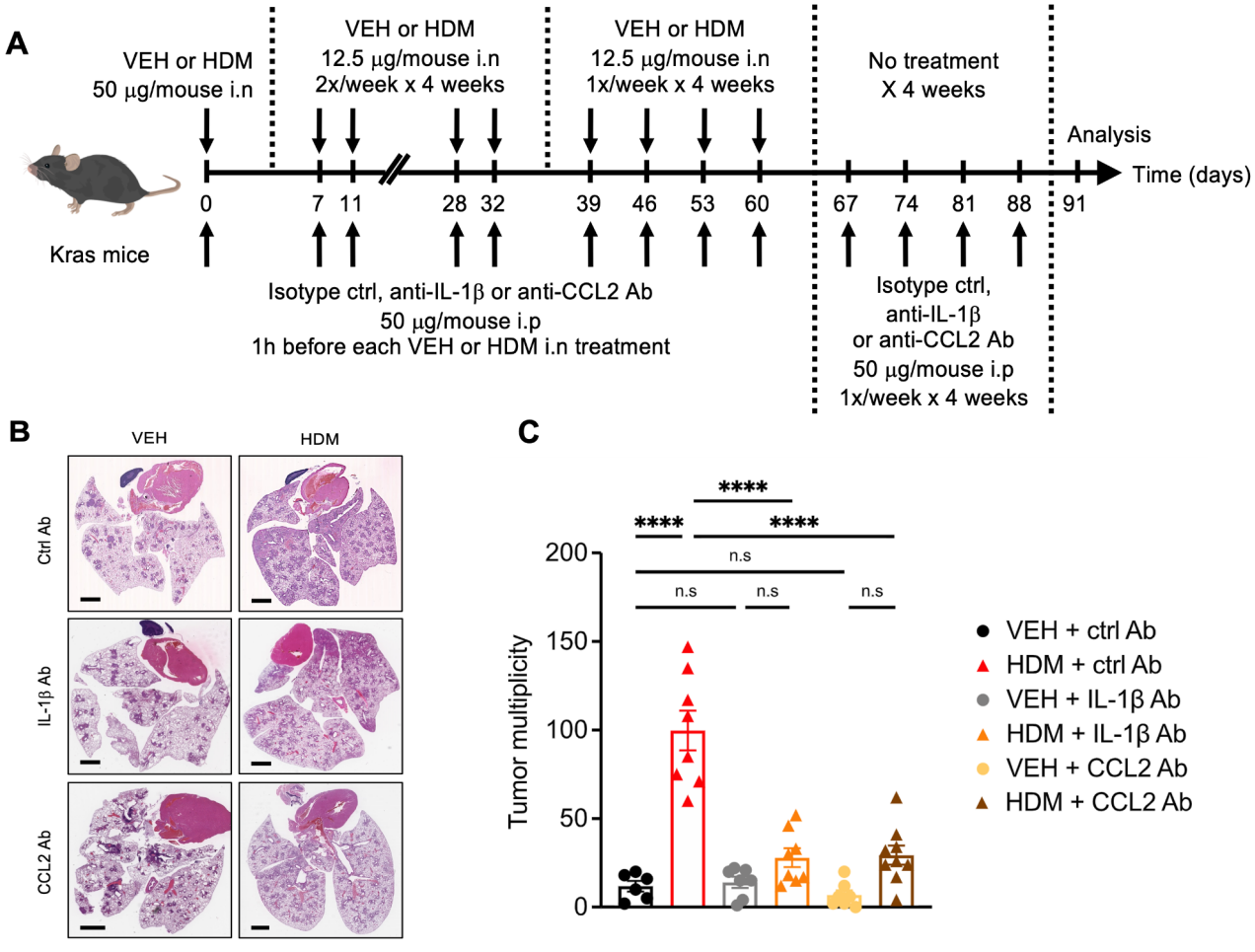

Figure 3: Neutralization of IL-1β or CCL2 inhibited the lung cancer-promoting effect of HDM A) Five-week-old *Kras*^{G12D} mice were randomly assigned to 6 groups and were treated i.n with VEH or HDM and i.p with a neutralizing anti-IL-1β, anti-CCL2, or with the isotype control (ctrl) antibody (Ab) as indicated in this schematic overview of the study design. **B)** Representative pictures of H&E-stained lung sections of *Kras*^{G12D} mice treated i.n with VEH or HDM and i.p with a neutralizing anti-IL-1β, anti-CCL2, or with the isotype control (ctrl) antibody (Ab) as shown in Figure S5A. VEH + ctrl Ab (n = 6), HDM + ctrl Ab (n = 8), VEH + IL-1β Ab (n = 7), and HDM + IL-1β Ab (n = 8), VEH + CCL2 Ab (n = 7), and HDM + CCL2 Ab (n = 9). Scale bars, 2 mm. **C)** Tumor multiplicity calculated on H&E-stained sections as shown in B. Data are presented as mean ± SEM. Statistical significance was assessed by one-way ANOVA with post hoc Bonferroni's test. (n.s: not significant, **** $P < 0.0001$).

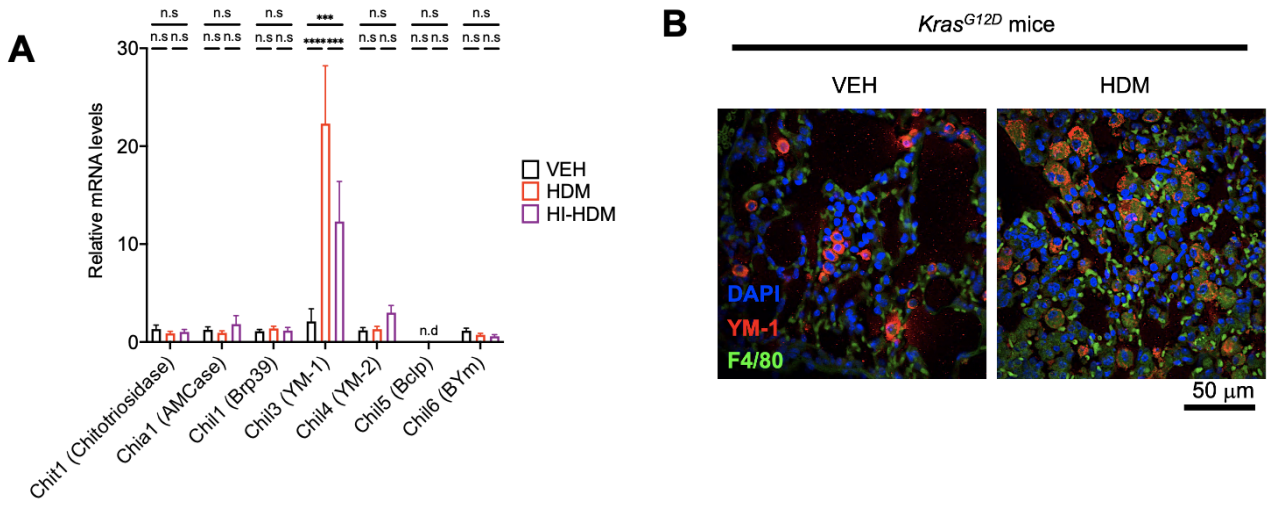

Figure 4: Long-term exposure to HDM induces the accumulation of YM-1 mRNA and protein in the lungs of *Kras*^{G12D} mice A) qPCR analysis of mouse chitinase and chitinase-like proteins in *Kras*^{G12D} mice treated with VEH, HDM, or HI-HDM as in Fig. 1A. **B)** Immunofluorescent staining of lung sections from *Kras*^{G12D} mice treated with VEH or HDM as in Fig. 1A, showing increased infiltration of cells (macrophages) co-expressing the markers F4/80 (green) and YM-1 (cherry).

Long-term exposure to HDM leads to the accumulation of YM-1 chitinase-like protein in the lungs of *Kras*^{G12D} mice

Studies have shown that HDM is a potent activator of Th2 immune responses to cause lung airway inflammation [6]. Recent studies have also found an association between chitinase and chitinase-like protein (CLPs) abnormalities in mouse models where Th2-related cytokines are overexpressed in the lungs [7,12]. Since chitin is a major target of these chitinases and CLPs, as well as a significant component of the HDM exoskeleton, we decided to look at the expression of chitinases and CLPs in the lungs of VEH and HDM-treated *Kras*^{G12D} mice to understand if chitinase or CLP overexpression could lead to inflammation. To evaluate our hypothesis, we performed a gene expression screen of the major chitinases and CLPs using lung tissue homogenates from the *Kras*^{G12D} mice from the cohort in Fig 1. HDM treatment led to an increase

in the expression of YM-1, a prominent CLP, in the lungs of the *Kras*^{G12D} mice compared to that of the control mice (Fig 4A). The effect of HDM on other chitinases or CLPs was not observed. While the expression of YM-1 was lower in the HI-HDM-treatment mice than in the ones treated with HDM, approximately 50% of the effect of HDM was preserved. This data suggests that the heat-insensitive components of HDM impact chitinase and CLP expression in the lung tissues.

To understand the effect of YM-1 in the lung space of the HDM-treated mice, we performed immunofluorescent staining on the lung sections of the *Kras*^{G12D} mice treated with HDM or VEH from the cohort in Fig 1 to observe YM-1 and macrophage activity. The number of macrophage cells, as well as cells staining for YM-1, increased in both number and size in the HDM-treated mice compared to the control (Fig 4B). There was also an increase in the colocalization of macrophages and YM-1 which suggests an association between macrophages and YM-1 in HDM-treated mice. Interestingly, these observations are from *Kras*^{G12D} mice that received their last intranasal HDM treatment 4 weeks before the lung tissue was extracted, thus showing that long-term HDM exposure leads to persistent recruitment of macrophages and upregulation of YM-1 in the lungs.

Chitin of HDM causes accelerates tumor progression in a mutant *Kras*-driven LC mouse model *Kras*^{G12D}

Based on our data that heat-insensitive components of HDM also significantly contribute to activating the IL-1β signaling pathway in the lungs of HI-HDM treated *Kras*^{G12D} mice as well as macrophages, and lead to an upregulation of YM-1 CLPs in HDM-treated mice, we wanted to assess the contribution of the heat-insensitive components of HDM. Chitin, a major component of the HDM exoskeleton as well as a moiety that is a target for various chitinases and CLPs, is an

extremely robust substance that can withstand temperatures up to 252 degrees Celsius [33]. Therefore, we identified chitin as a potential target of interest and wanted to evaluate the effect that chitin might have on tumor progression in a *Kras*^{G12D}-driven LC model.

To test our hypothesis, we treated *Kras*^{G12D} mice intranasally with pure chitin beads or polystyrene beads (both 5000 beads/30μL) as a control for 9 weeks and evaluated the occurrence of both lung inflammation as well as lung tumors in the groups at 18 weeks of age, 4 weeks after their last intranasal treatment (Fig 5A). We use control beads that are the same size (90 μm) as the chitin beads to ensure that the tumor response was not due to the size of the beads. Gross examination of the lungs showed that the lungs of the chitin-treated mice were found to be larger and heavier than that of the control mice (Fig 5B). As observed in previous experiments upon administration of VEH or HDM (Fig 1 and 3), *Kras*^{G12D} mice treated with either chitin or polystyrene beads developed predominantly alveolar/bronchiolar hyperplasia and adenomas. However, the number of lung lesions, as well as the tumor area, were significantly increased in mice treated with chitin beads as compared to those treated with control beads (Fig 5D and 5E).

To confirm these results, we treated another cohort of *Kras*^{G12D} mice intranasally with a powdered form of chitin sourced from shrimp exoskeleton (50 μg/30μL) or VEH (PBS) for 9 weeks and evaluated the occurrence of both lung inflammation as well as lung tumors in the groups at 18 weeks of age, 4 weeks after their last intranasal treatment (Fig 6A). Similar to the data from the mice treated with chitin beads, the lungs of the chitin solubilized powder-treated mice also appeared to be larger than those of the control mice and indicated inflammation (Fig 6B). The H&E-stained lung sections also found the chitin-treated mouse to have increased tumor multiplicity with the tumors covering a significantly larger area when compared to the VEH-treated mice (Fig 6D and 6E). Collectively, these results suggest that chronic exposure to

two different forms of chitin (beads or solubilized powder) leads to increased lung inflammation and accelerates the progression of the lung lesions in a *Kras*^{G12D}-driven mouse model.

Figure 5: Chronic intranasal instillation of Chitin beads accelerates lung tumor development in a *Kras^{G12D}*-driven lung cancer model. A) Five-week-old *Kras^{G12D}* mice were randomly assigned to two groups and were treated intranasally (i.n) with polystyrene control beads (n = 9) or chitin beads (n = 7) for 9 weeks as indicated in this schematic overview of the study design. At 18 weeks of age and 4 weeks after the last i.n challenge, the mice were sacrificed and the lungs were harvested. **B)** Representative pictures of the lungs (dorsal view) of control- and chitin-treated mice. Scale bars, 0.25 cm. **C)** Representative pictures of H&E-stained lung sections in the two experimental groups. The lower panels are the same images as the above panels after tumor area quantification using QuPath software. The area within the red borders was considered positive for lung tumors. The right panels show the boxed region (ROI#1) at higher magnification with areas of epithelial hyperplasia. Scale bars, 1 mm (whole lungs), 200 μm (ROI#1). **D)** Tumor multiplicity (i.e., number of lung lesions per mouse) calculated on H&E-stained sections as shown in D upper panels. **E)** Tumor area (i.e., the sum of lesion surface areas per mouse) calculated on H&E-stained sections as shown in D lower panels. Data are presented as mean ± SEM. Statistical significance was assessed by two-tailed Student's t-test. ** $P < 0.01$, **** $P < 0.0001$.

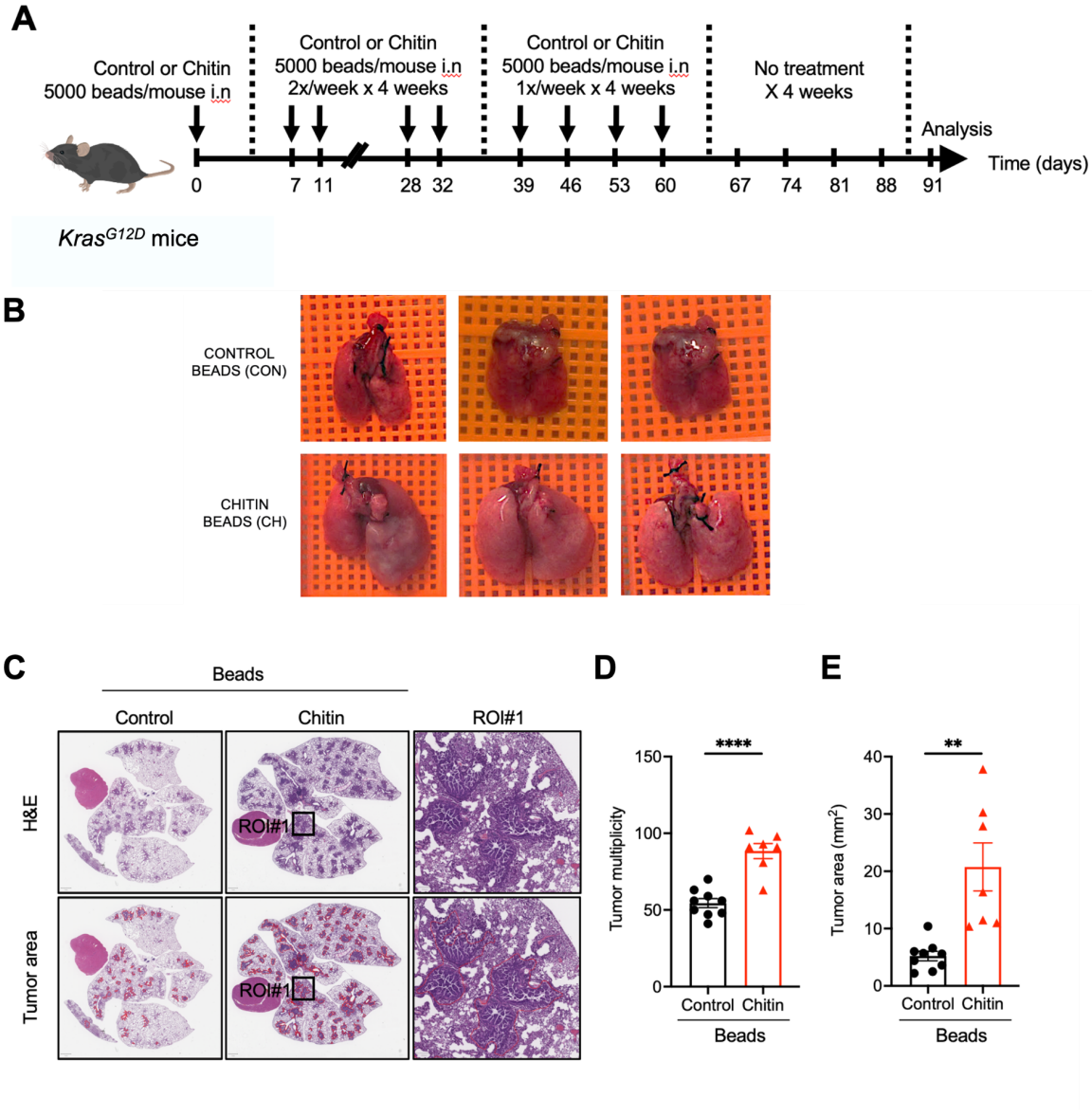
A
Control or Chitin
5000 beads/mouse i.n
Control or Chitin
5000 beads/mouse i.n
2x/week x 4 weeks
Control or Chitin
5000 beads/mouse i.n
1x/week x 4 weeks
No treatment
X 4 weeks
Analysis
Time (days)
0
7
11
28
32
39
46
53
60
67
74
81
88
91
Kras^G12D mice
B
CONTROL
BEADS (CON)
CHITIN
BEADS (CH)
C
Beads
Control
Chitin
ROI#1
H&E
Tumor area
ROI#1
D
Tumor multiplicity
****
150
100
50
0
Control
Chitin
Beads
E
Tumor area (mm2)
**
40
30
20
10
0
Control
Chitin
Beads

Figure 6: Chronic intranasal instillation of Chitin solubilized powder accelerates lung tumor development in a *Kras*^{G12D}-driven lung cancer model. A) Five-week-old *Kras*^{G12D} mice were randomly assigned to two groups and were treated intranasally (i.n) with control PBS (n = 8) or chitin (n = 9) for 9 weeks as indicated in this schematic overview of the study design. At 18 weeks of age and 4 weeks after the last i.n challenge, the mice were sacrificed and the lungs were harvested. **B)** Representative pictures of the lungs (dorsal view) of control- and chitin-treated mice. Scale bars, 0.25 cm. **C)** Representative pictures of H&E-stained lung sections in the two experimental groups. The lower panels are the same images as the above panels after tumor area quantification using QuPath software. The area within the red borders was considered positive for lung tumors. The right panels show the boxed region (ROI#1) at higher magnification with a papillary adenoma. Scale bars, 1 mm (whole lungs), 100 μm (ROI#1). **D)** Tumor multiplicity (i.e., number of lung lesions per mouse) calculated on H&E-stained sections as shown in D upper panels. **E)** Tumor area (i.e., the sum of lesion surface areas per mouse) calculated on H&E-stained sections as shown in D lower panels. Data are presented as mean ± SEM. Statistical significance was assessed by two-tailed Student's t-test. ** P <0.01.

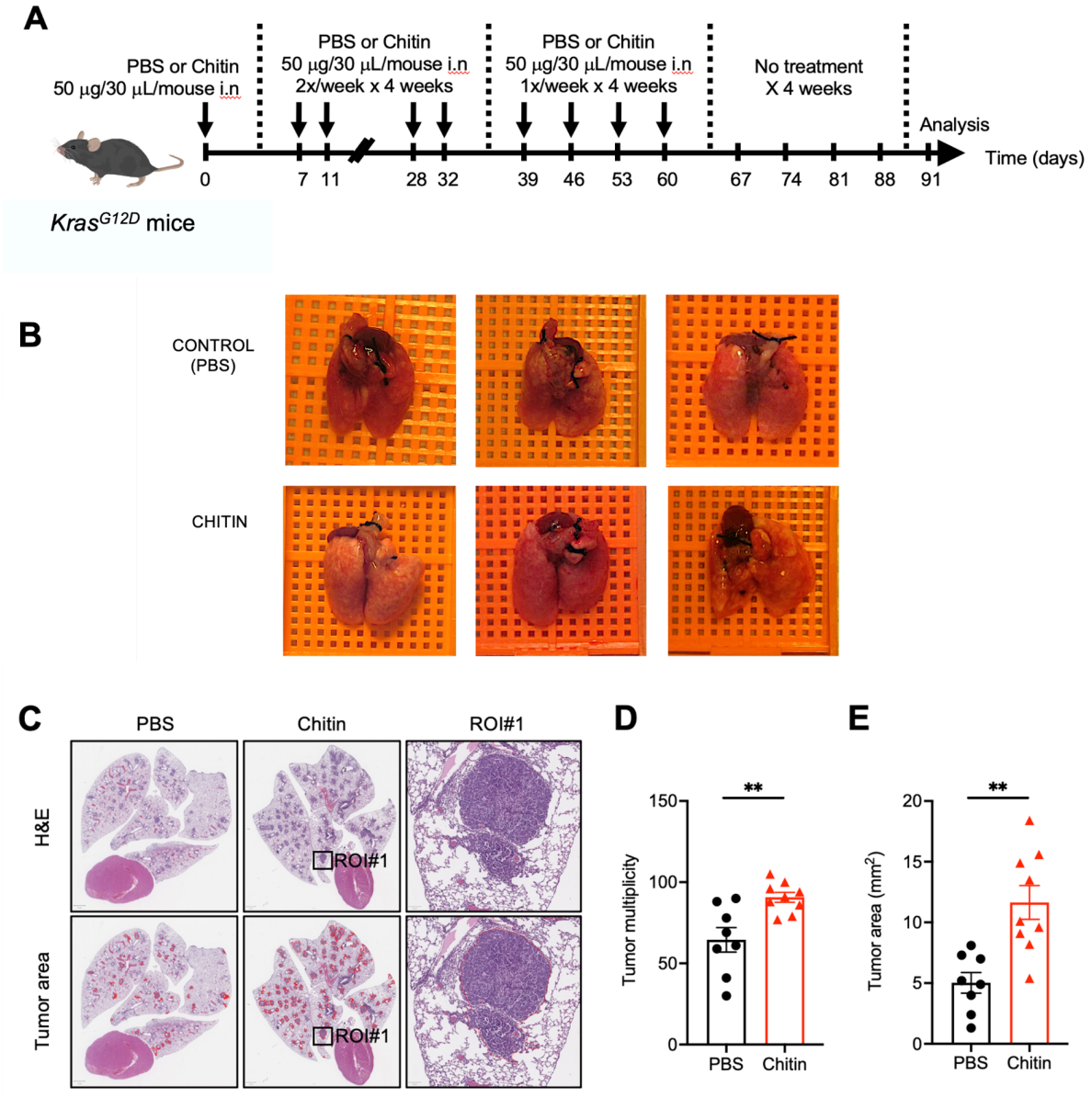
A
PBS or Chitin
50 µg/30 µL/mouse i.n
PBS or Chitin
50 µg/30 µL/mouse i.n
2x/week x 4 weeks
PBS or Chitin
50 µg/30 µL/mouse i.n
1x/week x 4 weeks
No treatment
X 4 weeks
Analysis
Time (days)
0
7
11
28
32
39
46
53
60
67
74
81
88
91
KrasG12D mice
B
CONTROL
(PBS)
CHITIN
C
PBS
Chitin
ROI#1
H&E
Tumor area
ROI#1
D
Tumor multiplicity
150
100
50
0
**
PBS
Chitin
E
Tumor area (mm2)
20
15
10
5
0
**
PBS
Chitin

Exposure to chitin activates the IL-1β signaling pathway in mouse macrophages

Based on our previous data that HDM activates the IL-1β signaling pathway in macrophages and as a result creates a pro-inflammatory pro-tumor microenvironment, and the data that shows the ability of chitin to accelerate tumor progression in the lungs of two separate chitin-treated of $Kras^{G12D}$ mice, we hypothesized that like HDM, chitin also causes inflammation by activating the NLRP3 mediated IL-1β signaling pathway in macrophages. To test our hypothesis, we conducted *in vitro* cell-based assays with primary BMDMs as well as RAW264.7 macrophages. We isolated BMDMs from WT C57BL/6 mice and stimulated them for 24h with HDM, varying concentrations of chitin beads, or VEH (PBS) in the presence or absence of extracellular ATP (to replicate the two priming steps to activate NLRP3), and IL-1β secretion in the supernatants was measured by ELISA (Fig 7A). Similar to the observation in HDM-treated BMDMs, stimulation with chitin led to an increase in IL-1β production in the culture supernatants in a concentration-dependent manner, (Fig 7B). As expected, IL-1β production increased significantly once ATP was added to the culture to complete the second priming step, although chitin alone was able to induce some IL-1β in a concentration-dependent manner.

To confirm the data generated with BMDMs, we repeated the experiment in RAW 264.7 macrophages. Cells were seeded into 24-well plates and stimulated for 24 hours with LPS, chitin beads or control beads, and ATP was added to each well for the last hour of culture, IL-1β secretion in the supernatants was measured by ELISA (Fig 7C). As observed with BMDMs, chitin also induced IL-1β in a concentration-dependent manner in RAW 264.7 cells. Interestingly, the concentration-dependent response in RAW 264.7 cells was stronger than that observed in the BMDMs (Fig 7D). The control beads led to negligible IL-1β production, which further verifies that the response observed is due to chitin and not the size of the beads. Collectively, this data suggests that chitin acts as a PAMP capable to stimulate the production of

IL-1β by macrophages (Fig 8), which consequently could create a lung microenvironment conducive to tumor formation and progression.

Acknowledgments

Figure 1 is currently being prepared for submission for publication of the material. Wang, Dong-Jie; Ganguly, Sneha; Bertin, Samuel. “Chronic Exposure to House Dust Mites Accelerates Lung Cancer Progression in Mice by Activating the NLRP3/IL-1β Pathway in Lung Macrophages.” The thesis author was the co-author of this material.

Figure 2 is currently being prepared for submission for publication of the material. Wang, Dong-Jie; Ganguly, Sneha; Bertin, Samuel. “Chronic Exposure to House Dust Mites Accelerates Lung Cancer Progression in Mice by Activating the NLRP3/IL-1β Pathway in Lung Macrophages.” The thesis author was the co-author of this material.

Figure 3 is currently being prepared for submission for publication of the material. Wang, Dong-Jie; Ganguly, Sneha; Bertin, Samuel. “Chronic Exposure to House Dust Mites Accelerates Lung Cancer Progression in Mice by Activating the NLRP3/IL-1β Pathway in Lung Macrophages.” The thesis author was the co-author of this material.

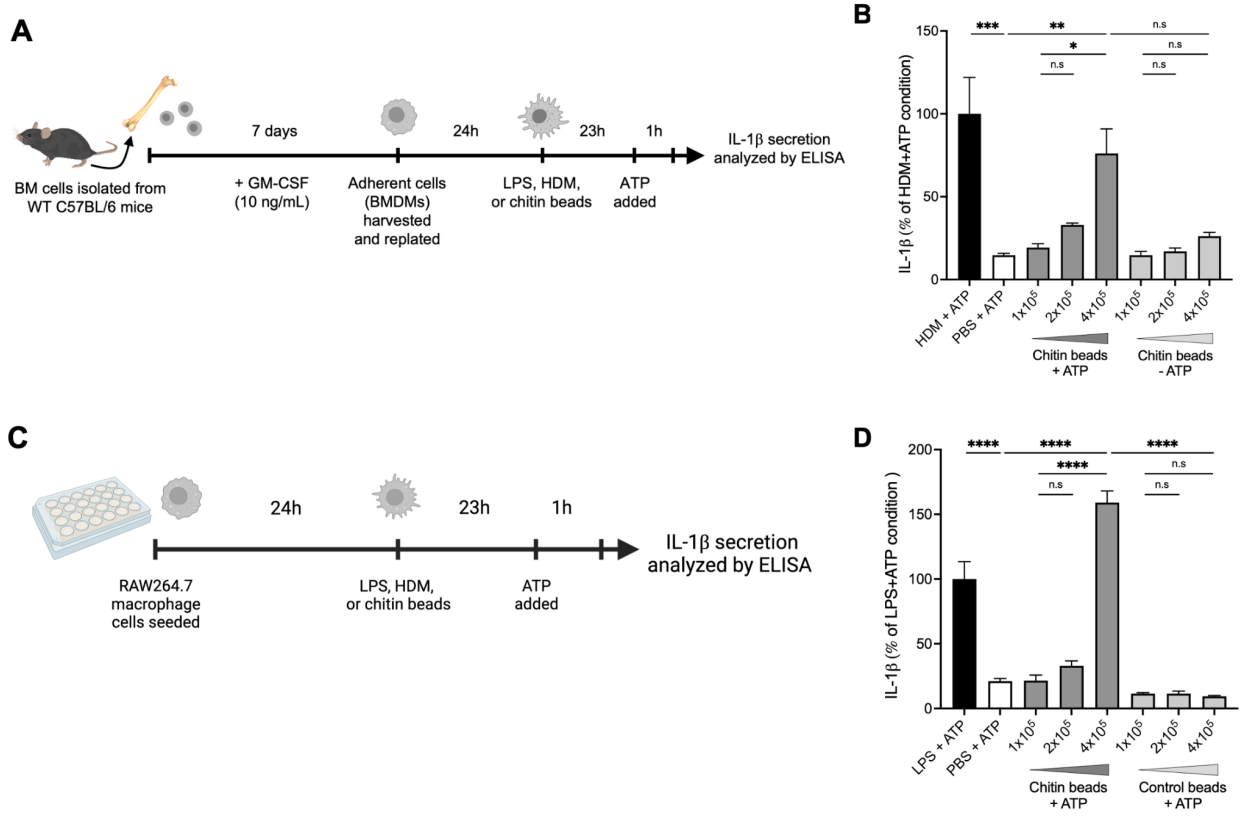

Figure 7: Chitin induces IL-1β in murine macrophages in a concentration-dependent manner. A) Schematic overview of the BMDM culture system. Bone marrow (BM) cells were harvested from wild-type (WT) mice and were differentiated into bone marrow-derived macrophages (BMDMs) in presence of granulocyte-macrophage colony-stimulating factor (GM-CSF) for 7 days. BMDMs were then stimulated for 24 hours with LPS, HDM, chitin beads, and ATP was added to each well for the last hour of culture. The supernatants were collected and the level of IL-1β in the supernatants was analyzed by ELISA. **B)** BMDMs were isolated and were stimulated for 24 hours by HDM (200 µg/mL), Chitin beads (1-4x10^5 beads), or PBS. ATP (5 mM) was added to some of the wells in the last hour of culture and the supernatant was collected and the level of IL-1β in the supernatants was analyzed by ELISA **C)** Schematic overview of the RAW264.7 culture system. Cells were seeded into 24 well plates and stimulated for 24 hours with LPS, HDM, chitin beads, or control beads, and ATP was added to each well for the last hour of culture. The supernatants were collected and the level of IL-1β in the supernatants was analyzed by ELISA. **D)** RAW264.7 cells were stimulated for 24 hours by HDM (200 µg/mL), Chitin beads, and control beads (1-4x10^5 beads), or PBS. ATP (5 mM) was added to the wells in the last hour of culture and the supernatant was collected and the level of IL-1β in the supernatants was analyzed by ELISA. Data are presented as mean ± SEM. Statistical significance was assessed by one-way ANOVA with post hoc Bonferroni's test. (n.s: not significant, * $P < 0.05$, ** $P < 0.01$, *** $P < 0.001$, ****$P < 0.0001$).

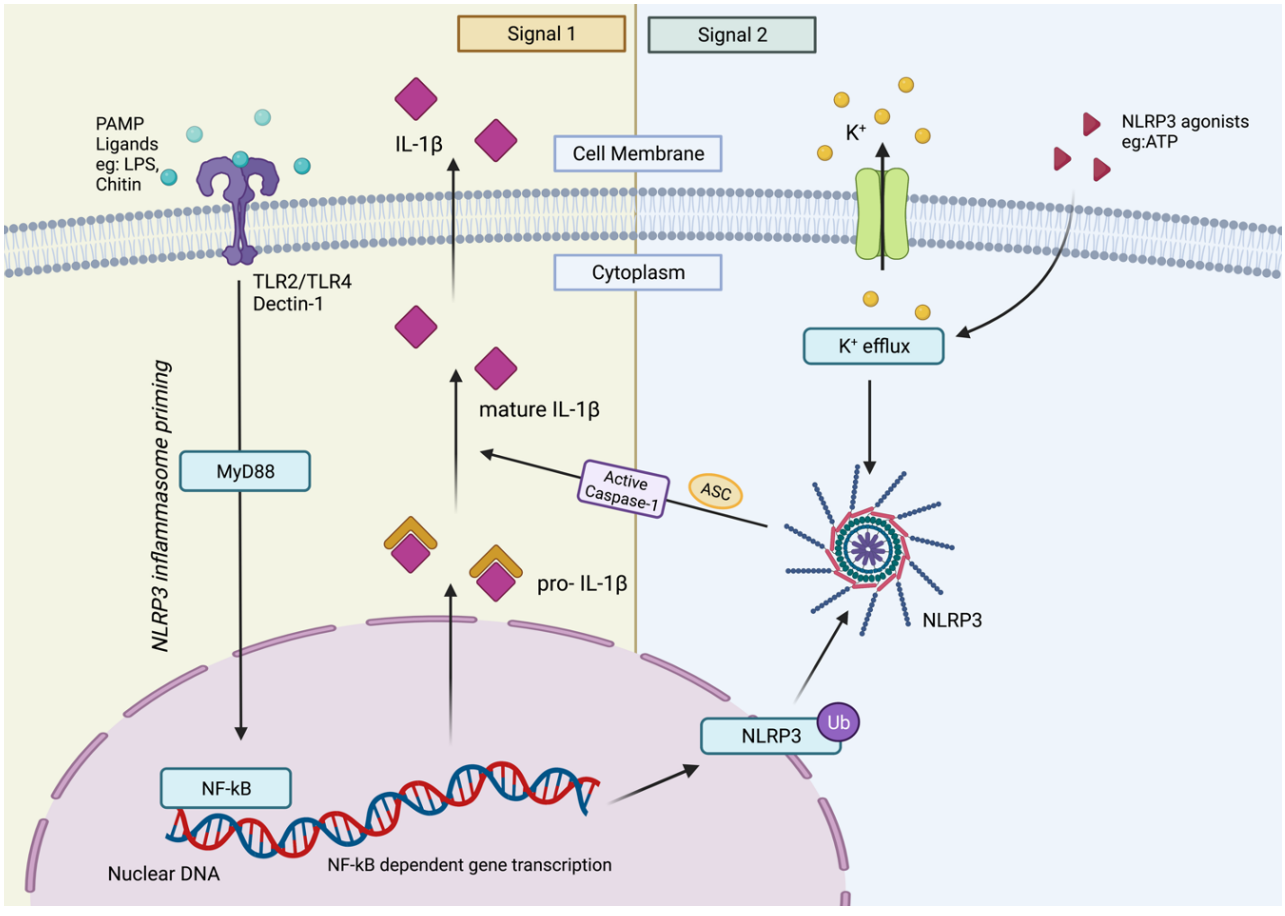

Figure 8: Proposed model of the effect of Chitin on IL-1β production by macrophages. Schematic diagram showing two-step priming of the NLRP3 inflammasome. The schematic representation was created with BioRender.com.

DISCUSSION

Although the link between chronic inflammation and cancer is well established, there remains a gap in our understanding of the exact mechanisms by which chronic inflammation promotes tumor development and progression. In this study, we aimed to fill this gap of knowledge by using chronic HDM exposure as a tool to provoke chronic lung inflammation and to create a model system that mimics the physiological response to prevalent environmental aeroallergens such as HDM, that continuously expose us to the robust polymer, chitin. We explored its impact on LC development in mice and identified a potential mechanism by which chitin-induced chronic lung inflammation may promote LC (Fig 8).

Our results reveal that chitin, an exoskeletal component of HDM, is a significant contributor to the ability of HDM to cause inflammation and accelerate lung tumor development and progression in a strain of mice genetically predisposed to develop LC (i.e., $Kras^{G12D}$ mice). Even though heat treatment of HDM was able to considerably reduce the effect of HDM on tumor progression and IL-1β production, approximately 50% of the effect was still preserved suggesting that heat-insensitive factors also contributed to these effects (Fig 1, 2B, 3A). Indeed, we observed that chitin, a major heat-insensitive component of HDM, was also able to provoke inflammation and tumor progression in $Kras^{G12D}$ mice *in vivo* and to activate the NLRP3/IL-1β signaling pathway in macrophages *in vitro* (Fig 5-7).

In our chitinase and CLP gene expression screen as well, we found an association between long-term HDM treatment and a significant upregulation of YM-1, a chitin-binding protein without any enzymatic properties (Fig 4A). YM-1 is known to remain in the lungs at sites of chronic inflammation and crystalizing in the tissue space without any evidence of being digested [26]. As a result, it is possible that chitin-bound YM-1 crystallization in the lungs could lead to further inflammation via alternative activation of macrophages and lead to tissue damage,

creating a tumor-prone microenvironment [27]. Although we expected to see an increase in AMCase levels due to increased chitin exposure in the lungs, our chitinase and CLP gene expression analysis did not reveal any significant increase in the levels of AMCase in the tissue of the mice. This unexpected result could be due to the timeline of the experiment where the lungs were harvested from the mice 4 weeks after the last intranasal treatment. This timeline is potentially a limitation in our study as the 18-week model allows us to observe the long-lasting effect of chitin on the lung microenvironment but not its short-term effects. Since previous studies have shown that AMCase is a short-term acting enzyme, which means its activity is short-lived, it is possible that an increased AMCase expression may be observed if the lungs are harvested within 24 hours of the last HDM treatment [12]. We also used chitin beads of 90 μm which are deemed too big to be phagocytosed by the macrophages. Therefore, understanding the effect of AMCase activity on chitin-induced inflammation will also provide an insight into the size-dependent effect of the chitin fragments on the tumor microenvironment.

Since the relationship between allergy and cancer has been a very controversial topic, widely discussed over the last few decades, an interdisciplinary field of Allergo-Oncology has emerged [28]. Several epidemiological studies have demonstrated an inverse, neutral, or positive association between allergy and lung cancer. The reason epidemiological studies are difficult to perform or conclude from is because of the multiple variables in the studies that are difficult to account for. For example, asthma was found to be protective against the risk of developing LC in some studies potentially because asthmatics tend to be non-smokers [29]. While asthma's relationship to LC continues to be controversial to this day, the recent discovery of differing asthma endotypes such as Th2/Th17-low and Th2/Th17-predominant, in which IL-1β plays a key role, may provide an explanation as to why it has been so difficult to establish an association [30]. Hopefully, these recent discoveries will help design future epidemiological studies that will

account for the heterogeneity of allergic diseases. Additionally, another caveat to this issue with epidemiological studies is that most asthmatic patients are also treated with inhaled corticosteroids (ICS), such as budesonide. Budesonide has anti-inflammatory and anti-proliferative properties which may considerably reduce the risk of developing LC. In a large study including 75,307 participants, adults with asthma had a 2.8-fold increased risk of developing LC, and treatment with a high cumulative dose of ICS was associated with a 56% risk reduction [31], suggesting that an inflammatory response mediates the link between asthma and LC. Moreover, in a previous study [32], we found that budesonide inhibits NLRP3 and decreases IL-1β production by macrophages, which could partly explain its anti-tumor effect. Thus, we can speculate that human subjects chronically exposed to HDM who do not develop asthma and therefore do not take ICS are more vulnerable to the LC-promoting effect of HDM. As a result, further studies are needed to test the effects of naturally occurring HDM and its active components, such as chitin, to determine whether long-term exposure could prove to be a risk factor for LC in humans. Moving forward, our results will help direct future research towards identifying the particular type of inflammation that is conducive to LC development and potentially identify new therapeutic strategies to prevent tumor development in patients with allergic asthma.

MATERIALS AND METHODS

Animals

Initial breeding pairs of CCSP^{Cre} (JAX, Strain# 036525) [33] and *LSL-Kras*^{G12D} (JAX, Strain# 008179) (64) mice, both on the C57BL/6 background, were a gift from Dr. Seon Hee Chang (The University of Texas MD Anderson Cancer Center). For the generation of *Kras*^{G12D} mice, CCSP$^{Cre+/-}$ mice were intercrossed with *LSL-Kras*$^{G12D+/-}$ as detailed below. All the mice were bred in our vivarium under specific pathogen-free (SPF) conditions for more than 6 months and were genotyped before they were used in any experiments. All the mice were kept on a 12-hour light, and 12-hour dark cycle with a standard chow diet and water. All the animal studies were conducted in accordance with protocols approved by the UCSD Institutional Animal Care and Use Committee (IACUC) and following the ARRIVE guidelines.

Allergen extract solubilization

HDM extracts were generated by Greer laboratories as follows: whole bodies of *Dermatophagoides pteronyssinus* were extracted with 0.01 M ammonium bicarbonate (1:20, w/v) overnight at 2-8°C. The crude extract, recovered after centrifugation, was dialyzed against pyrogen-free water, sterilized using a 0.22-µm membrane filter, and lyophilized under aseptic conditions. Lyophilized extracts of HDM (Cat# XPB82D3A2.5 or XPB82D3A25) were resuspended based on their total protein content at 2 mg/mL in sterile 0.9% sodium chloride solution (BD, Cat# 306546) for *in vivo* experiments or at 10 mg/mL in sterile PBS (Thermo Fisher Scientific, Cat# 14190144) for *in vitro* experiments, and were then aliquoted and stored at -80°C until used. When indicated, HDM was heat-inactivated (HI-HDM) for 1h at 95ºC as previously described [23].

Preparation of Chitin and Polystyrene Beads

Pure chitin beads (New England Biolabs NEB, Cat#S6651S) with size of approximately 90 μm diameters were prepared by filtering beads through a 100μm cell strainer (Millipore Sigma, Cat#CLS431752) and resuspended in sterile PBS (Thermo Fisher Scientific, Cat# 14190144) at a concentration of 1.6 x 10^5 beads per mL. 30 μL (5000 beads) of this suspension was intranasally administered to mice under light anesthesia (isoflurane) as previously described [8]. Polystyrene beads with a size standard of 90 μm (Polysciences Inc., Cat#07315-5) were prepared and administered to the mice as described above for chitin beads and were used as control.

Preparation of Chitin Powder

We obtained chitin powder obtained from shrimp shells (Sigma Aldrich, Cat#C7170) and solubilized them in pre-warmed PBS (Thermo Fisher Scientific, Cat# 14190144) at a concentration of 50ng/30μL. The mixture was sonicated at 25% power 5 times for 5 minutes alternating with 5-minute cooling periods to break up the larger fragments into smaller fragments. The solubilized powder was then collected after being filtered through a 100 μm filter. For intranasal treatments, the solution was aliquoted and stored at -20°C until used.

***Kras^{G12D}*-driven LC model**

We crossed the *LSL-Kras^{G12D}* strain [34], which carries a Lox-Stop-Lox (LSL) sequence followed by the *Kras^{G12D}* point mutation allele commonly associated with human cancer, with a transgenic mouse expressing the Cre recombinase under the control of the Clara cell secretory protein (CCSP) promoter [33], thereby allowing the expression of the mutant KRAS oncogenic

protein specifically in lung club cells (formerly known as Clara cells). The resulting $CCSP^{Cre+/-}$-$Kras^{G12D+/-}$ mice (hereafter referred to as $Kras^{G12D}$ mice) were treated i.n with HDM, HI-HDM, , or with the vehicle (VEH, 0.9% sodium chloride solution, BD, Cat# 306546) for a total of 9 or 13 weeks (from 5 weeks of age to 14 or 18 weeks of age, respectively). The mice were first sensitized i.n under light anesthesia (isoflurane) with HDM (DP, 50 µg/30 µL/mouse), HI-HDM (DP, 50 µg/30 µL/mouse, VEH (30 µL/mouse), chitin beads, polystyrene beads (5000 beads/30 µL), chitin solubilized powder or PBS (30 µL/mouse) on day 0, and were challenged one week later with HDM (DP, 12.5 µg/30 µL/mouse), HI-HDM (DP, 12.5 µg/30 µL/mouse), or VEH (30 µL/mouse), chitin beads, polystyrene beads (5000 beads/30 µL), chitin solubilized powder or PBS (30 µL/mouse) i.n twice a week for the first 4 weeks and once a week for the following 4 weeks. When indicated, mice were injected i.p for 9 weeks, 1h before each HDM or VEH i.n treatment, and then once a week for an additional 4 weeks, with either a neutralizing anti-mouse IL-1β Ab (BioXCell, Cat# BE0246), a neutralizing anti-mouse CCL2 Ab (BioXCell, Cat# BE0185) or with the isotype control Ab (BioXCell, Cat# BE0091). All Abs were diluted in *InVivo*Pure pH 7.0 Dilution Buffer (BioXCell, Cat# IP0070) and administrated at the same dose (50 µg/100 µL/mouse) and periodicity as previously described (35, 36). Finally, 4 weeks after the last i.n challenge and 72h after the last i.p injection (18-week-old time point), the mice were euthanized by CO2 asphyxiation and the BALF, and the lungs were harvested. After ligation, one lung lobe of the right lung was removed, snap-frozen in liquid nitrogen, and stored at -80°C until further processing. The remaining 4 lung lobes were fixed by intratracheal instillation and immersion in 10% buffered formalin solution for 24h and were stored in histological grade 70% ethanol until paraffin embedding.

Histological analysis

After fixation, the lung samples were brought in histological grade 70% ethanol to the UCSD Moores Cancer Center Tissue Technology Shared Resource for paraffin embedding and sectioning. The fixed lungs were cut into 4-6-µm sections, placed on glass slides, and stained with hematoxylin (Thermo Fisher Scientific, Cat# 7221) and eosin (Thermo Fisher Scientific, Cat# 7111) (H&E) on a Gemini AS slide stainer (Thermo Fisher Scientific) using standard staining procedures. H&E slides were scanned on a Hamamatsu Nanozoomer (Hamamatsu Photonics) or an Aperio AT2 slide scanner (Leica Biosystems), digitized, and whole-slide images were used for tumor assessments. Tumor count and tumor area was determined using QuPath software [38] software in a blinded fashion following expert guidance provided by two board-certified pathologists and current recommendations for the classification of proliferative pulmonary lesions in mice [39].

Immunofluorescence Staining and Confocal Microscopy

Immunohistofluorescence (IF) was performed using standard staining procedures as previously described [41]. Briefly, 4-6-µm mouse lung FFPE sections were cleared, dehydrated and antigen retrieval was performed in Antigen Unmasking Solution (Vector Labs, Cat# H-3301) at 95ºC for 30 min. Blocking was done using 3% donkey serum and 1% BSA in PBS 0.1% Triton X-100 for 30 min. The slides were then incubated with a goat anti-mouse YM-1 Ab (R&D Systems, Cat# AF2446, 1:50 dilution in blocking buffer) for 1h at RT, followed by detection with a donkey anti-goat IgG-Alexa Fluor 546 (Invitrogen, Cat# A11078, 1:500 dilution in blocking buffer) and with an Alexa Fluor 488 anti-mouse F4/80 Ab (BioLegend, Cat# 123120, 1:200 dilution in blocking buffer) for 1h at RT. Nuclear staining was done with Hoechst 33258

(Invitrogen, 50 ng/mL in PBS 0.1% Triton X-100) for 10 min at RT. Slides were rinsed with deionized water and mounted in ProLong Gold antifade reagent (Invitrogen). Finally, the fluorescence images were acquired using a 60x oil-immersion objective on a confocal laser-scanning microscope (Olympus IX81) with Fluoview software.

BMDM isolation and treatment

BMDMs were isolated from WT C57BL/6J (JAX, Strain# 000664) using standard protocols as previously described [42]. Briefly, harvested bone marrow cells were cultured for 6 days in RPMI medium supplemented with 10% FBS, L-Glutamine, 1× penicillin/streptomycin, and recombinant mouse GM-CSF (BioLegend, Cat# 576302, 10 ng/mL). After 6 days, the adherent cells were collected, re-plated at 1 x 10^6 cells per mL in 24-well plates and were allowed to adhere to the plates for 24h. BMDM ($CD11b^+F4/80^+$) purity was routinely checked by flow cytometry and was ~80% (data not shown). BMDMs were then incubated with indicated concentrations of HDM, HI-HDM, or LPS (Sigma-Aldrich, Cat# L2630, 100 ng/mL) or with chitin or polystyrene beads for 24h. ATP (Sigma-Aldrich, Cat# A7699, 5 mM) was added to each cell culture well for the last hour of incubation. Following these treatments, the supernatants were collected, and cytokine levels were assessed by ELISA. LPS+ATP was used as a positive control for NLRP3 activation and IL-1β release.

RAW264.7 cell treatment

RAW 264.7 cells (ATCC, Cat# TIB-71) were cultured in DMEM medium supplemented with 10% FBS and 1× penicillin/streptomycin and were treated as indicated above for BMDMs. For *in vitro* treatments, chitin and polystyrene beads were added to RAW264.7 and BMDM cell culture medias at serial concentrations of 1-4 x 10^5 beads per well in 24 well-plates.

ELISA

The levels of IL-1β in BMDM or RAW 264.7 cell culture supernatants, in the BALF, or in lung tissue homogenates were determined using a specific mouse IL-1β ELISA kit (R&D Systems, Cat# DY401-05) and following the manufacturers' instructions.

RT-qPCR analysis

Isolation of total RNA from lung tissues or BMDMs was carried out with the PureLink RNA Mini Kit (Thermo Fisher Scientific, Cat# 12183018A) following the manufacturer's protocol. One μg of RNA sample was used for reverse transcription (RT) and cDNA synthesis using qScript cDNA SuperMix (Quanta Biosciences, Cat# 95048). Quantitative real-time PCR (qPCR) was performed on a QuantStudio 3 Real-Time PCR System (Thermo Fisher Scientific, Cat# A28137) using PowerUp SYBR Green Master Mix (Thermo Fisher Scientific, Cat# A25742) according to the manufacturer's instructions. Samples were run in triplicate and normalized to *Krt19* or *Gapdh* gene expression as indicated in the figure legends. qPCR primers for specific target genes were designed based on their reported sequences and synthesized by Integrated DNA Technologies (IDT) Technologies. See oligonucleotide sequences are listed in the table below:

Table 1: Oligonucleotide sequences for qPCR primers for specific target genes

	Forward Primer	Reverse Primer
CHIL5 (Bclp)	5'-GTCTCCACTCCACACAACCAAC-3'	5'-TGGCTTCCAGTTCAAAAGCCT-3'
CHIL6 (BYm)	5'-TTCAACAACTGGCCTCAGCA-3'	5'-TCTCCGAAGTTCCAGCAACC-3'
CHIL4 (YM-2)	5′-GCAAGGCCTCTTATCGAGGG-3′	5′-TCCATGGAAGCATGATGCAGA-3′
CHIL3 (YM-1)	5'-ACCTGCCCCGTTCAGTGCCAT-3'	5'-CCTTGGAATGTCTTTCTCCACAG-3'
CHIA1 (AMCase)	5′-TGGACCTGGACTGGGAATACC-3′	5′-TGGGCCTGTTGCTCTCAATAG- 3′
CHIT1 (Chitotriosidase)	5′-TGGGCAGGTGTGATGACTCT-3′	5′-CCCTGGGAAAGAACCGAACTG-3′
CHIL1(Brp39; Chi311)	5′-CAGACGCCATCCAACCTTTC-3′	5′-TTTCCACCCTCCAACAGACA-3′

Graphical illustrations

Graphical illustrations were created using BioRender (https://biorender.com) and Servier Medical Art (https://smart.servier.com).

Statistics

Both male and female mice were used in this study. The effects reported were observed in a sex-independent manner and were similar in single- and co-housed mice. Age- and sex-matched mice were randomly assigned to treatment groups. Sample sizes for *in vivo* studies were determined based on preliminary studies and the variability of the LC models used. All animal studies were adequately powered to achieve statistically significant results with the smallest number of animals. The number of mice per group and the level of replication for each *in vitro* and *in vivo* experiment is mentioned in the figure legends. Graphical representations

were generated using Prism (GraphPad Software) and data are presented as mean ± SEM. The statistical significance between two groups was determined using unpaired Student t-tests with two-tailed *P*-values. The statistical significance between more than two groups was determined using one- or two-way analysis of variance (ANOVA) with post hoc Bonferroni's tests. *P*-values of less than 0.05 were considered statistically significant. All statistics were computed using Prism (GraphPad Software).

REFERENCES

1. Torre LA, Siegel RL, Ward EM, Jemal A. 2016. Global Cancer Incidence and Mortality Rates and Trends--An Update. Cancer Epidemiol Biomarkers Prev. 25:16-27.

2. Brown DW, Young KE, Anda RF, Giles WH. 2005. Asthma and risk of death from lung cancer: NHANES II Mortality Study. J Asthma. 42:597-600

3. Lambrecht BN, Hammad H (2012) The airway epithelium in asthma. Nat Med 18(5): 684–692.

4. Hubaux R, Becker-Santos DD, Enfield KS, Lam S, Lam WL, Martinez VD. 2012. Arsenic, asbestos and radon: emerging players in lung tumorigenesis. Environ Health. 11:89.

5. Malhotra J, Malvezzi M, Negri E, La Vecchia C, Boffetta P. 2016. Risk factors for lung cancer worldwide. Eur Respir J. 48:889-902.

6. Gregory LG, Lloyd CM (2011) Orchestrating house dust mite-associated allergy in the lung. Trends Immunol 32(9):402–411

7. Lee CG, Da Silva CA, Lee JY, Hartl D, Elias JA (2008) Chitin regulation of immune responses: An old molecule with new roles. Curr Opin Immunol 20(6):684–689.

8. Van Dyken, S. J., Liang, H.-E., Naikawadi, R. P., Woodruff, P. G., Wolters, P. J., Erle, D. J., & Locksley, R. M. (2017). Spontaneous Chitin Accumulation in Airways and Age-Related Fibrotic Lung Disease. Cell, 169(3), 497-509.e13.

9. Wang D, Li W, Albasha N, Griffin L, Chang H, Amaya L, Ganguly S, Zeng L, Keum B, Gonzalez-Navajas JM, Levin M, AkhavanAghdam Z, Snyder H, Schwartz D, Tao A, Boosherhri LM, Hoffman HM, Rose M, Estrada MV, Varki N, Herdman S, Corr M, Webster NJG, Raz E, and Bertin S. Long-Term Exposure to House Dust Mites Accelerates Lung Cancer Development in Mice. Manuscript submitted for publication.

10. Kim, L. K., Morita, R., Kobayashi, Y., Eisenbarth, S. C., Lee, C. G., Elias, J., … Flavell, R. A. (2015). AMCase is a crucial regulator of type 2 immune responses to inhaled house dust mites. Proceedings of the National Academy of Sciences, 112(22), E2891–E2899.

11. Miller, J. D. (2018). The Role of Dust Mites in Allergy. *Clinical Reviews in Allergy & Immunology*, *57*(3), 312–329. https://doi.org/10.1007/s12016-018-8693-0

12. Przysucha, N., Górska, K., & Krenke, R. (2020). Chitinases and Chitinase-Like Proteins in Obstructive Lung Diseases – Current Concepts and Potential Applications. *International Journal of Chronic Obstructive Pulmonary Disease*, *Volume 15*, 885–899.

13. Elieh Ali Komi D, Sharma L, Dela Cruz CS. Chitin and Its Effects on Inflammatory and Immune Responses. *Clinical Reviews in Allergy & Immunology*. 2017;54(2):213-223. doi:10.1007/s12016-017-8600-0

14. Vannella, K. M., Ramalingam, T. R., Hart, K. M., de Queiroz Prado, R., Sciurba, J., Barron, L., Wynn, T. A. (2016). Acidic chitinase primes the protective immune response to gastrointestinal nematodes. Nature Immunology, 17(5), 538–544.

15. Zhang, J.-M., & An, J. (2007). Cytokines, Inflammation, and Pain. *International Anesthesiology Clinics*, *45*(2), 27–37.

16. Lin, Y., Xu, J., & Lan, H. (2019). Tumor-associated macrophages in tumor metastasis: biological roles and clinical therapeutic applications. *Journal of Hematology & Oncology*, *12*(1).

17. Cassel, S. L., & Sutterwala, F. S. (2010). Sterile inflammatory responses mediated by the NLRP3 inflammasome. *European Journal of Immunology*, *40*(3), 607–611. https://doi.org/10.1002/eji.200940207

18. Latz, E., Xiao, T. S., & Stutz, A. (2013). Activation and regulation of the inflammasomes. *Nature Reviews Immunology*, *13*(6), 397–411. https://doi.org/10.1038/nri3452

19. Greten, F. R., & Grivennikov, S. I. (2019). Inflammation and Cancer: Triggers, Mechanisms, and Consequences. *Immunity*, *51*(1), 27–41.

20. Moghaddam, S. J., Li, H., Cho, S.-N., Dishop, M. K., Wistuba, I. I., Ji, L., Kurie, J. M., Dickey, B. F., & Demayo, F. J. (2009). Promotion of lung carcinogenesis by chronic obstructive pulmonary disease-like airway inflammation in a K-ras-induced mouse model. American Journal of Respiratory Cell and Molecular Biology, 40(4), 443–453.

21. Meuwissen, R., & Berns, A. (2005). Mouse models for human lung cancer. Genes & Development, 19(6), 643–664.

22. Johnson, J. R., Wiley, R. E., Fattouh, R., Swirski, F. K., Gajewska, B. U., Coyle, A. J., Gutierrez-Ramos, J.-C., Ellis, R., Inman, M. D., & Jordana, M. (2004). Continuous exposure to house dust mite elicits chronic airway inflammation and structural remodeling. American Journal of Respiratory and Critical Care Medicine, 169(3), 378–385.

23. Post, S., Nawijn, M. C., Hackett, T. L., Baranowska, M., Gras, R., van Oosterhout, A. J. M., & Heijink, I. H. (2012). The composition of house dust mite is critical for mucosal barrier dysfunction and allergic sensitisation. Thorax, 67(6), 488–495.

24. Moossavi, M., Parsamanesh, N., Bahrami, A., Atkin, S. L., & Sahebkar, A. (2018). Role of the NLRP3 inflammasome in cancer. Molecular Cancer, 17(1), 158.

25. Kelley, N., Jeltema, D., Duan, Y., & He, Y. (2019). The NLRP3 Inflammasome: An Overview of Mechanisms of Activation and Regulation. International Journal of Molecular Sciences, 20(13).

26. Harbord, M., Novelli, M., Canas, B., Power, D., Davis, C., Godovac-Zimmermann, J., … Segal, A. W. (2002). Ym1 Is a Neutrophil Granule Protein That Crystallizes in p47 -deficient Mice. *Journal of Biological Chemistry*, *277*(7), 5468–5475.

27. Zhu, W., Lönnblom, E., Förster, M., Johannesson, M., Tao, P., Meng, L., … Holmdahl, R. (2020). Natural polymorphism of Ym1 regulates pneumonitis through alternative activation of macrophages. *Science Advances*, *6*(43).

28. della Valle, L., Gatta, A., Farinelli, A., Scarano, G., Lumaca, A., Tinari, N., Cipollone, F., Paganelli, R., & di Gioacchino, M. (2020). Allergooncology: an expanding research area. Journal of Biological Regulators and Homeostatic Agents, 34(2), 319–326.

29. Takiguchi, H., Takeuchi, T., Niimi, K., Tomomatsu, H., Tomomatsu, K., Hayama, N., Oguma, T., Aoki, T., Urano, T., Asai, S., Miyachi, H., & Asano, K. (2018). Proportion and clinical characteristics of non-asthmatic non-smokers among adults with airflow obstruction. PloS One, 13(5), e0196132.

30. Liu, W., Liu, S., Verma, M., Zafar, I., Good, J. T., Rollins, D., Groshong, S., Gorska, M. M., Martin, R. J., & Alam, R. (2017). Mechanism of TH2/TH17-predominant and neutrophilic TH2/TH17-low subtypes of asthma. The Journal of Allergy and Clinical Immunology, 139(5), 1548-1558.e4.

31. Woo, A., Lee, S. W., Koh, H. Y., Kim, M. A., Han, M. Y., & Yon, D. K. (2021). Incidence of cancer after asthma development: 2 independent population-based cohort studies. The Journal of Allergy and Clinical Immunology, 147(1), 135–143.

32. Dong, L., Zhu, Y.-H., Liu, D.-X., Li, J., Zhao, P.-C., Zhong, Y.-P., Chen, Y.-Q., Xu, W., & Zhu, Z.-Q. (2019). Intranasal Application of Budesonide Attenuates Lipopolysaccharide-Induced Acute Lung Injury by Suppressing Nucleotide-Binding Oligomerization Domain-Like Receptor Family, Pyrin Domain-Containing 3 Inflammasome Activation in Mice. Journal of Immunology Research, 2019, 7264383.

33. Li, H., Cho, S. N., Evans, C. M., Dickey, B. F., Jeong, J.-W., & DeMayo, F. J. (2008). Cre-mediated recombination in mouse Clara cells. *Genesis*, *46*(6), 300–307.

34. Jackson, E. L., Willis, N., Mercer, K., Bronson, R. T., Crowley, D., Montoya, R., … Tuveson, D. A. (2001). Analysis of lung tumor initiation and progression using conditional expression of oncogenic *K-ras*. *Genes & Development*, *15*(24), 3243–3248.

35. Coffelt, S. B., Kersten, K., Doornebal, C. W., Weiden, J., Vrijland, K., Hau, C.-S., … de Visser, K. E. (2015). IL-17-producing γδ T cells and neutrophils conspire to promote breast cancer metastasis. *Nature*, *522*(7556), 345–348.

36. Teng, K.-Y., Han, J., Zhang, X., Hsu, S.-H., He, S., Wani, N. A., … Ghoshal, K. (2017). Blocking the CCL2–CCR2 Axis Using CCL2-Neutralizing Antibody Is an Effective Therapy for Hepatocellular Cancer in a Mouse Model. *Molecular Cancer Therapeutics*, *16*(2), 312–322.

37. Kalidhindi, R. S. R., Ambhore, N. S., & Sathish, V. (2020). Cellular and Biochemical Analysis of Bronchoalveolar Lavage Fluid from Murine Lungs. *Methods in Molecular Biology*, 201–215.

38. Bankhead, P., Loughrey, M. B., Fernández, J. A., Dombrowski, Y., McArt, D. G., Dunne, P. D.,Hamilton, P. W. (2017). QuPath: Open source software for digital pathology image analysis. *Scientific Reports*, *7*(1).

39. Nikitin, A. Yu., Alcaraz, A., Anver, M. R., Bronson, R. T., Cardiff, R. D., Dixon, D., … Travis, W. D. (2004). Classification of Proliferative Pulmonary Lesions of the Mouse. *Cancer Research*, *64*(7), 2307–2316.

40. de Jong, P. R., Taniguchi, K., Harris, A. R., Bertin, S., Takahashi, N., Duong, J., … Raz, E. (2016). ERK5 signalling rescues intestinal epithelial turnover and tumour cell proliferation upon ERK1/2 abrogation. *Nature Communications*, *7*(1).

41. Lee, J., Kim, T. H., Murray, F., Li, X., Choi, S. S., Broide, D. H.,Raz, E. (2015). Cyclic AMP concentrations in dendritic cells induce and regulate Th2 immunity and allergic asthma. *Proceedings of the National Academy of Sciences*, *112*(5), 1529–1534.